◆ Human Brain Mapping 34:2464–2483 (2013) ◆

Can Spherical Deconvolution Provide More Information Than Fiber Orientations? Hindrance Modulated Orientational Anisotropy, a True-Tract Specific Index to Characterize White Matter Diffusion

Flavio Dell'Acqua,[1,2]* Andrew Simmons,[1,2,3] Steven C.R. Williams,[1,2] and Marco Catani[1,4]

[1]*Department of Neuroimaging, King's College London, Institute of Psychiatry, United Kingdom*
[2]*NIHR Biomedical Research Centre for Mental Health at South London and Maudsley NHS Foundation Trust and Institute of Psychiatry, King's College London, United Kingdom*
[3]*MRC Centre for Neurodegeneration Research, King's College London, Institute of Psychiatry, United Kingdom*
[4]*Natbrainlab, Department of Forensic and Neurodevelopmental Sciences, King's College London, Institute of Psychiatry, United Kingdom*

Abstract: Diffusion tensor imaging (DTI) methods are widely used to reconstruct white matter trajectories and to quantify tissue changes using the average diffusion properties of each brain voxel. Spherical deconvolution (SD) methods have been developed to overcome the limitations of the diffusion tensor model in resolving crossing fibers and to improve tractography reconstructions. However, the use of SD methods to obtain quantitative indices of white matter integrity has not been extensively explored. In this study, we show that the hindrance modulated orientational anisotropy (HMOA) index, defined as the absolute amplitude of each lobe of the fiber orientation distribution, can be used as a compact measure to characterize the diffusion properties along each fiber orientation in white matter regions with complex organization. We demonstrate that the HMOA is highly sensitive to changes in fiber diffusivity (e.g., myelination processes or axonal loss) and to differences in the microstructural organization of white matter like axonal diameter and fiber dispersion. Using simulations to describe diffusivity changes observed in normal brain development and disorders, we observed that the HMOA is able to identify white matter changes that are not detectable with conventional DTI indices. We also show that the HMOA index can be used as an effective threshold for in vivo data to improve tractography reconstructions and to better map white matter complexity inside the brain. In conclusion, the HMOA represents a true tract-specific and sensitive index and provides a compact characterization of white matter diffusion properties with potential for widespread application in normal and clinical populations. *Hum Brain Mapp* 34:2464–2483, 2013. © 2012 Wiley Periodicals, Inc.

Contract grant sponsor: Biomedical Research Centre for Mental Health at South London and Maudsley NHS Foundation Trust and Institute of Psychiatry, King's College London.

*Correspondence to: Flavio Dell'Acqua, NATBRAINLAB, Department of Neuroimaging and NIHR Biomedical Research Centre, Institute of Psychiatry, PO 89, King's College London, De Crespigny Park, London SE5 8AF, United Kingdom.
E-mail: flavio.dellacqua@kcl.ac.uk

Received for publication 28 June 2011; Revised 28 January 2012; Accepted 14 February 2012
DOI: 10.1002/hbm.22080
Published online 5 April 2012 in Wiley Online Library (wileyonlinelibrary.com).

© 2012 Wiley Periodicals, Inc.

Key words: diffusion imaging; crossing fibers; spherical deconvolution; hindrance modulated orientational anisotropy; tractography; NuFO

INTRODUCTION

In the last two decades, magnetic resonance diffusion imaging has offered a unique opportunity to probe the microstructural integrity of the living human brain. Its applications range from characterization of brain development across the lifespan to quantification of brain degeneration in vascular and neurological disorders [Jones, 2008]. Average properties of tissues within each voxel can be characterized by diffusion indices, such as fractional anisotropy (FA) and mean diffusivity (MD) using the classical tensor model [Basser et al., 1994; Pierpaoli et al., 1996] or the generalized FA (GFA) and similar indices for more complex methods like q-Ball [Tuch, 2004] or diffusion spectrum imaging [Wedeen et al., 2005]. These indices are generally thought to describe the microstructural properties of tissues in normal and pathological brains. For example, decreased MD during early brain development is interpreted as an indication of increased myelination of white matter fibers [Dubois et al., 2008], whereas a decrease in FA, for example in multiple sclerosis, is usually indicative of white matter demyelination [Beaulieu, 2002]. These indices are useful in research and clinical practice but their interpretation is not always straightforward. One of the major limitations is that these indices represent average measures of tissue properties. For voxels containing one type of tissue (e.g., parallel fibers of the mid-sagittal corpus callosum), the values of these indices are specific only to that tissue. However, when the voxel contains more than one fiber population, or a mix of different tissues (e.g., white matter fibers and grey matter), the indices are degraded by partial volume effect and, therefore, are no longer fiber- or tissue-specific. A classical example is neurodegeneration along a white matter tract which crosses with an unaffected fiber tract. In voxels containing both the degenerating and the normal fibers, the FA may increase as result of degeneration of the perpendicular fibers [Wheeler-Kingshott and Cercignani, 2009]. Other approaches based on multicompartmental models try to directly fit the diffusion signal from High Angular Resolution Diffusion Imaging (HARDI) or from multishell *b*-value data. Although multiple *b*-value approaches may provide extremely useful information to disentangle the characteristics of multiple tissues, these techniques are currently not easily transferable to clinical populations [Alexander et al., 2010; Assaf and Basser, 2005; Wedeen et al., 2005; Wu and Alexander, 2007]. Moreover, a common limitation of multiparametric fitting approaches is that the increased complexity of the models sometimes restricts the ability to provide consistent results across a range of configurations, including regions of pathology. Here, fitting errors, due to inadequate model selection, may extend to multiple parameters making the clinical or biological interpretation of the results not always straightforward.

Spherical deconvolution (SD) has been recently developed to resolve multiple fiber orientations and is based on a relatively simple model of signal generation. Instead of fitting a finite number of parameters, it tries to estimate a continuous 3D distribution of the possible fiber orientations. SD is based on the assumption that the signal from different white matter bundles can be described by a common and characteristic three-dimensional signal profile, the fiber response function [Anderson, 2005; Tournier et al., 2004]. Deconvolving diffusion signals with a chosen fiber response function allows the estimation of the weight of each fiber bundle distributed across the angular space (e.g., the fibers randomly distributed within a spherical space) to the total diffusion signal within each voxel. The result of the deconvolution operation is the fiber orientation distribution (FOD), a spherical function whose multipeak shape provides information on the number of distinct fiber orientations, their orientation, and the weight of each fiber component. This model has proved to be effective for the extraction of multiple fiber orientations in complex white matter regions where high angular resolution is required to resolve multiple crossing [Alexander, 2005; Dell'Acqua et al., 2007; Jian and Vemuri, 2007; Kaden et al., 2008; Sakaie and Lowe, 2007; Tournier et al., 2007]. Furthermore, current SD acquisition sequences are close to standard diffusion tensor imaging (DTI) protocols and can, therefore, be easily incorporated in clinical research protocols.

Different approaches have been proposed to resolve the SD model and recent algorithms have shown increased stability to noise and partial volume effect [Alexander, 2005; Dell'Acqua et al., 2010; Jian and Vemuri, 2007; Kaden et al., 2008; Tournier et al., 2007]. Preliminary approaches to tractography based on SD have also been reported [Dell'Acqua et al., 2008; Jeurissen et al., 2010a; Pannek et al., 2010]. However, the potential to quantify white matter changes with SD has not been extensively explored. In the following sections, we describe how SD can be used to develop novel quantitative indices specific to single fiber (or tissue) components. A direct comparison with classical voxel-specific indices (e.g., FA and MD) is then presented using simulated normal and pathological data. Applications to improve the quantification of the number of distinct fiber orientations and tractography reconstructions of complex white matter regions on in vivo data are

presented. Relevant clinical uses and potential limitations are finally discussed.

METHODS

Theory

Fiber response function and fiber signals

SD is based on the main assumption that the signal from each fiber component is modeled by the chosen fiber response function. However, such a hypothesis should be considered as only partially correct for signals measured from biological tissues. Differences in the microstructural organization of white matter (WM) bundles affect the diffusion properties of each fiber. In particular, different levels of myelination, axonal density or even axonal radius are known to be important factors that modulate the radial diffusivity in WM tracts [Assaf et al., 2008; Barazany et al., 2009; Beaulieu, 2002]. The effect of different diffusion properties on the measured MR signal can be inferred by modeling the signal from a single fiber as [Anderson, 2005]

$$E(\theta) = e^{-b(\lambda \cos^2\theta + \beta \sin^2\theta)} \quad (1)$$

where $E(\theta)$ is the diffusion weighted MR signal normalized to the nondiffusion weighted signal; λ and β represent the diffusivity along and perpendicular to the direction of the fiber, θ is the angle between the diffusion gradient and the fiber orientation, and b is the b-value. This equation is based on the classical Gaussian diffusion model and the fiber signal corresponds to an axial symmetric tensor whose eigenvalues are [λ β β] [Hsu and Mori, 1995; Wiegell et al., 2000]. Equation (1) shows how the signal E changes according to generic apparent diffusion coefficients of λ and β. However, using more complex diffusion models, it is also possible to relate the attenuation of the diffusion signal directly to specific WM microstructural features. In particular, assuming statistical independence of the net displacement of water molecules along the axis and the radial direction of the fiber, the signal from a single fiber can be modeled as [Assaf et al., 2004]:

$$E(\boldsymbol{q}, \tau) = E_{\parallel}(\boldsymbol{q}_{\parallel}, \tau) E\perp(\boldsymbol{q}\perp, \tau) \quad (2)$$

where $E_{\parallel}(\boldsymbol{q}_{\parallel},\tau)$ is the signal attenuation along the axis of the fiber bundle and is usually modeled as free 1D-Gaussian diffusion. $E\perp(\boldsymbol{q}\perp,\tau)$ is the signal attenuation measured perpendicularly to the fiber orientation which can be described by using models of restricted diffusion, such as, the van Gelderen model [van Gelderen et al., 1994] or the multiple correlation function (MCF) approach introduced by Grebenkov [2007]. The advantage of these models is that, taking into account the finite duration of the diffusion gradient pulses, it is possible to directly relate the diffusion signal attenuation with WM microscopic features such as axonal diameter [Alexander et al., 2010; Assaf et al., 2008]. Here, $\boldsymbol{q}_{\parallel}$ and $\boldsymbol{q}\perp$ are the components of the $\mathbf{q}$-vector decomposed along the parallel and the perpendicular direction of the fiber, where $|\boldsymbol{q}| = \gamma\delta G$ and $\tau = \Delta - \delta/3$ is the diffusion time, with γ the gyromagnetic ratio, G is the maximum amplitude of the diffusion gradients, δ is the duration of the diffusion gradients, and Δ is the time interval between these gradients [Assaf et al., 2004].

Figure 1 shows an example of the changes in the 2D fiber signal profile with increasing radial diffusivity [Eq. (1)] and axonal radius [Eq. (2)] obtained with a diffusion gradient configuration achievable with a clinical setup. For the diffusion models described by Eqs. (1) and (2), an increase in the radial diffusivity or axonal radius produces a substantial attenuation of the whole signal. However, after normalization to their maximum (to remove all scaling factors), the signal profiles show minimal variation in shape for small radial diffusivity ($<0.5 \times 10^{-3}$ mm^2/s) and for axonal radii ranging from 0.01 to 10 μm, a range that corresponds to normal histological values measured in the human brain [Aboitiz et al., 2003; Waxman et al., 1995]. For higher radial diffusivities ($>0.5 \times 10^{-3}$ mm^2/s) or axonal radii larger than 10 μm, the figure also shows that differences in the shape of the fiber signal become apparent.

In these examples, therefore, most of the differences in the signal profile can be associated with the scaling factor, but for increasing radial diffusivities or larger axons, changes in the shape also need to be taken into account. Moreover, it can also be verified that numerically, the Gaussian and the restricted diffusion models adopted in these examples provide identical (using van Gelderen) or almost identical (using MCF) results if, for each axonal radius, the corresponding apparent Gaussian radial diffusivity is applied to Eq. (1). Thus, to a first approximation, both signal profiles can be described by a more general geometric relation as:

$$E(\theta) = k e^{-b\alpha \cos^2\theta} \quad (3)$$

where k is a term that controls the scaling factor and α is a term that controls the shape of the fiber signal profile. This expression is equivalent to Eq. (1) if we set $k = \exp(-b\beta)$ as a term that describes the radial hindrance of the fiber and $\alpha = \lambda - \beta$ to characterize the anisotropy of the fiber signal profile [Dell'Acqua et al., 2007].

In the rest of the article, we investigate how variations in the fiber signal (i.e., shape and scaling factors) affect SD and propose new indices to quantify and characterize white matter changes directly from the FOD profile.

Effect of different fiber signal profiles on the FOD

Previous SD studies have shown that the presence of crossing fibers with different diffusion properties affects the amplitude rather than the orientation of the

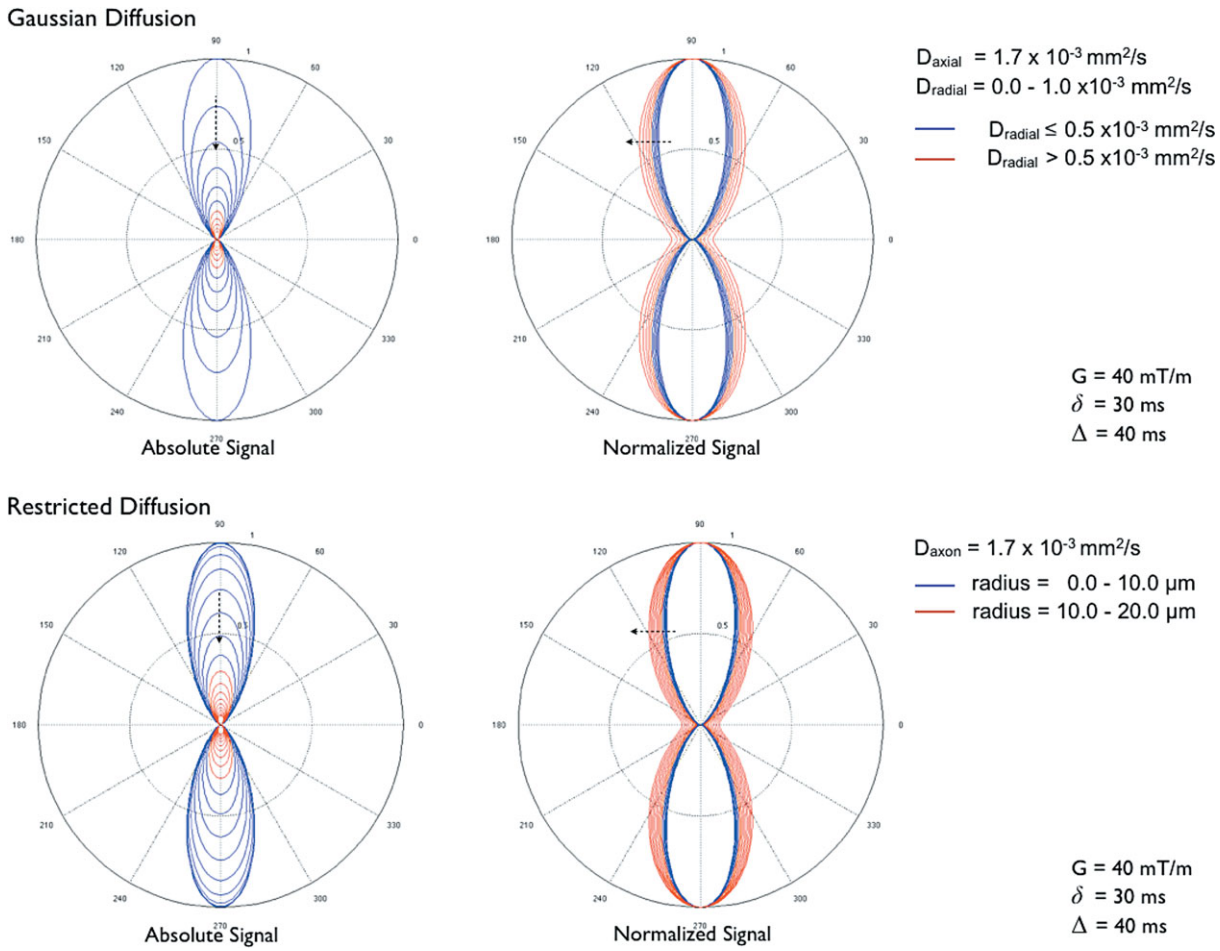

Figure 1.

Two-dimensional signal profile changes for a fiber described using models of Gaussian diffusion and restricted diffusion inside a cylinder. On the left, signal changes are displayed as absolute signal changes. On the right, signal profiles are normalized to the maximum value to remove all scaling factors and highlight only shape differences. Black arrows indicate the direction of changes for increase radial diffusivity or radius. Simulation parameters are shown in figure legend.

corresponding FOD components [Anderson, 2005; Dell'Acqua et al., 2007; Tournier et al., 2004]. Here, we analyze in detail how these variations in both scaling factor and shape parameters affect the amplitude and other characteristics of the FOD.

First, if we consider only differences in scaling factor between the fiber signal and the fiber response function, the linear relationship of the convolution model guarantees that scaling factors in the fiber signal are directly transformed into scaling factors in the corresponding FOD components. Hence, increases in radial diffusivity decrease the term k and, consequently, the amplitude of the corresponding FOD peak decreases.

Figure 2a shows an example of a fiber with a range of scaling factors crossing with a fixed fiber. As k decreases, the amplitude of the corresponding FOD component decreases while the amplitude of the FOD lobe of the fixed fiber remains constant.

Less obvious and more difficult to quantify is the effect of deconvolving fiber signals with different shape profiles or, more generally, in the presence of mismatch between the measured fiber signals and the chosen fiber response function. If we first consider a fiber signal S which is perfectly deconvolved with a sharper (higher α) fiber response function, H, a solution, R, can always be obtained that satisfies

$$S = H \otimes R \tag{4}$$

However, it can be verified that here R is not the impulse function that would be obtained by deconvolving with the exact fiber response function, but rather a smoother axial

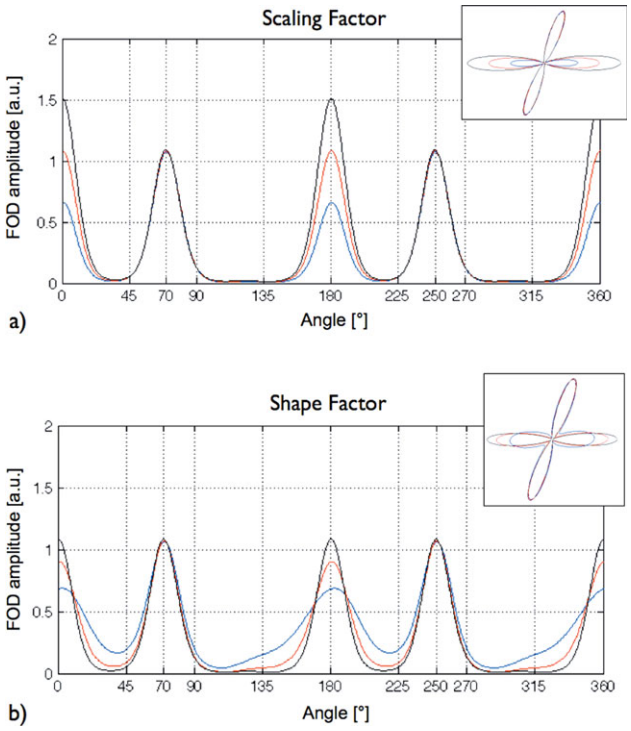

Figure 2.

Example of 2D FOD profiles for a simulated fiber-crossing configuration where diffusion properties are changed in one of the two fibers (FOD lobes at 0° and 180°) and kept constant in the second fiber (FOD lobes at 70° and 250°). In (**a**), the effect of decreasing the scaling factor are shown for $k = 0.7$ (black), $k = 0.5$ (red), and $k = 0.3$ (blue). The scaling factor of the second fiber is $k = 0.5$, whereas the shape factor for both fibers is always equal to $\alpha = 1.5 \times 10^{-3}$ mm^2/s. In (**b**), the effect of decreasing shape factors are shown with $\alpha = 1.5$ (black), $\alpha = 1.2$ (red), and $\alpha = 0.7$ (blue) $\times 10^{-3}$ mm^2/s. For the second fiber, α is fixed to 1.5×10^{-3} mm^2/s, whereas the scaling factor of both fibers is equal to 0.5. In the examples, the *b*-value was equal to 3000 s/mm^2, the fiber response characterized by a shape factor of $\alpha = 2.0 \times 10^{-3}$ mm^2/s and the crossing angle equal to 70°.

symmetric profile centered along the direction of the fiber. Similar to a Gaussian bell-shape deconvolved with a sharper Gaussian, R can be considered as a residual blurring that remains on the ideal impulsive FOD. Therefore, deconvolving with a sharper fiber response will produce smoother FOD lobes depending on how close or far signals are to the chosen fiber response. In the presence of crossing configurations with fibers described by different shape profiles, the final FOD can, therefore, also be described as the sum of a mixture of residual R_i functions such as

$$S = H \otimes R_1 + H \otimes R_2 = H \otimes (R_1 + R_2) = H \otimes \mathrm{FOD} \qquad (5)$$

In clinical terms, this suggests that in the presence of a tissue with decreased anisotropy the recovered FOD components will not only be reduced by the scaling factor due to the increase of the radial diffusion component but also by the decreased shape factor α that will produce an increased blurring of the corresponding FOD components. Figure 2b shows as an example a fiber with changes only in its shape factor crossing with a fixed fiber. For different shape factors of the fiber, the amplitude of the corresponding FOD components decrease and the whole lobe becomes smoother as α decreases.

In practice, it must be noted that all SD methods proposed in the literature already recover FOD profiles as spherical functions with rounded lobes rather than true impulse functions even when the exact fiber response function is applied. These rounded lobes can also be considered as an additional angular blurring that always affects the deconvolved FOD independently of the chosen fiber response function. This blurring is normally required to regularize the ill-conditioned nature of the deconvolution problem and originates, for example, from the truncation of higher spherical harmonic orders [Anderson, 2005; Tournier et al., 2004, 2007], the chosen number of iterations of the deconvolution algorithm [Dell'Acqua et al., 2007] or, more simply, from the introduction of additional regularization terms [Kaden et al., 2008; Sakaie and Lowe, 2007].

It is important to observe that, as a consequence, differences between the fiber response and the measured fiber signal, therefore, modulate the overall blurring of the corresponding FOD lobe. Although a sharper fiber response introduces additional blurring, the choice of a fiber response with a profile smoother than the actual fiber (i.e., lower α) produces the opposite effect by "eroding" part of the blurring. In more detail, with a rounder profile, the fiber response weights some of the signal components of the fiber more strongly. In this situation, however, signal contributions from one fiber may also be erroneously included by the larger fiber response in other FOD lobes, potentially affecting their amplitude, orientation, or angular resolution. A precise quantification of this effect is hard to determine because it depends not only on the chosen fiber response function but also on the intrinsic blurring that is specific to the deconvolution algorithm used. In this study, therefore, we perform numerical simulations to quantify these effects as well as the effects of fibers with different diffusion properties using a SD algorithm that we recently developed to provide high angular resolution and noise stability within a clinical research acquisition scenario [Dell'Acqua et al., 2010]. Similar results are also expected for other SD methods.

Amplitude of the FOD peaks and hindrance modulated orientational anisotropy

From the examples in the previous section, we can observe that changes in fiber signal are always translated into changes in the amplitude of the specific FOD lobe. Moreover, in a certain range of conditions, these

amplitudes can also be considered independent or minimally affected by changes in the amplitude of other FOD lobes within the same voxel. In other words, the FOD not only provides relative information about the proportion of the lobe amplitudes in each voxel but also gives an absolute measure that reflects the specific diffusion properties along each fiber orientation. As we have shown in the previous sections, this amplitude depends not only on the fiber volume fractions but also on the radial diffusion hindrance of the particular white matter orientation (i.e., the scaling factor k) and on the anisotropy of the fiber signal profile (i.e., the shape term, α). Because FOD profiles also do not require min-max normalization to enhance fiber orientations as required by other HARDI approaches, the amplitude of each FOD lobe is an absolute value that remains comparable across different voxels and brain regions. This is also true in the presence of partial volume with isotropic compartments (gray matter, cerebrospinal fluid (CSF), or edema), where the reduced volume fraction of the fiber compartments is reflected in reduced amplitude of the fiber orientations.

The absolute amplitude of each FOD lobe can, therefore, be used to detect and quantify diffusion or anisotropy changes along specific white matter orientations. For this reason, we define the absolute amplitude of each FOD lobe normalized to a reference amplitude as an index of hindrance modulated orientational anisotropy (HMOA). Here, normalization is only required to define the index within a range from zero and one. In particular, by selecting as reference the highest FOD amplitude that can be realistically measured in a biological sample, an HMOA with a value of one corresponds to a signal equivalent to the reference fiber, whereas an HMOA of zero corresponds to the absence of a fiber.

The reference signal can be defined as the signal corresponding to a condition of totally anisotropic diffusion defined by a tensor equal to $[2\ 0\ 0] \times 10^{-3}$ mm^2/s. By choosing no radial diffusivity, we select the maximum scaling factor (i.e., $k = 1$) that can be found on a fiber signal and consequently on the corresponding lobe amplitude. Different profiles or shapes of the reference fiber signal can be chosen by changing only the corresponding α value to match the characteristics of the studied biological system (e.g., in vivo, postmortem, etc.). Here, an axial diffusivity equal to 2.0×10^{-3} mm^2/s gives the most anisotropic signal profile and also represents the upper limit of diffusivity we can expect to measure in vivo in white matter.

Potential applications of the HMOA

The HMOA as defined above offers clear advantages over FA or GFA. First, the HMOA can be used as an indirect index to describe the microstructural properties specific to single fiber populations. This is particularly useful in conditions where a voxel contains multiple fiber orientations with different biological properties (e.g., axonal diameter, degree of myelination, etc.). A direct application is, for example, the characterization of the maturation of specific tracts in the developing brain or the quantification of degeneration of fibers in pathological conditions.

Another possible application is the use of the HMOA as an effective threshold to mask small amplitude and spurious FOD lobes that originate from noise or from partial volume effect in isotropic tissue. The HMOA is an absolute measure that is directly related with diffusion MR signal of each fiber components. Hence, when compared with other methods that set mask thresholds as a proportion of the maximum amplitude of each FOD or orientation distribution function (ODF), a mask threshold defined using the HMOA value provides a constant threshold across brain regions independently of the FOD amplitude of each individual voxel. In this study, we provide two examples of how the application of HMOA values as thresholds can be used to better quantify the number of fiber orientations or to improve tractography reconstruction.

Number of fiber orientation maps

SD methods can also provide information about the complexity of white matter organization in the human brain by looking at the number of distinct fiber orientations within each voxel. The number of fiber orientation (NuFO) maps are usually estimated as the number of local maxima of the FOD profile in each voxel [Dell'Acqua et al., 2009; Jeurissen et al., 2010b; Nedjati-Gilani et al., 2006] and can be visualized as maps where the gray scale intensity of each voxel corresponds to the number of fibers [Behrens et al., 2007]. Here, we propose to improve the estimation of the NuFO maps by using the additional information provided by the HMOA index to threshold and exclude spurious components. A two-threshold approach is applied here. A first "absolute" threshold based on the HMOA value is used to exclude small local maxima due to noise and isotropic tissue [Dell'Acqua et al. 2010]. In this study, different values of the HMOA threshold are compared using multiples of the amplitude of a spherical FOD obtained from an isotropic voxel of gray matter ($D = 0.7 \times 10^{-3}$ mm^2/s) as a reference amplitude (A_{iso}). A second "relative" threshold, equivalent to a chosen percentage of the maximum lobe amplitude, is applied to remove remaining local maxima with value greater than the absolute threshold, but whose value is relatively small compared with the maximum amplitude of the corresponding FOD. This additional threshold is necessary only in those FODs with the highest amplitude (e.g., in the corpus callosum) where ringing-like components, usually of negligible amplitude, may be higher than the absolute threshold.

Tractography

Recent studies have shown that tractography algorithms based on multifiber methods may overcome some of the

limitations of the classical tensor model [Behrens et al., 2007; Berman et al., 2008; Wedeen et al., 2008]. In particular, SD gives information on the orientation of different fiber bundles within the same region that can improve tractography reconstructions in regions containing complex white matter organization. An example of the advantage of SD tractography is the ability to identify trajectories in regions with crossing fibers such as the corpus callosum, the association pathways and the cortico-spinal tracts (CSTs) where diffusion tensor tractography often produces false negatives (e.g., failure to reconstruct real pathways). However, tractography based on multifiber methods can be biased toward false positive reconstructions by showing artifactual tracts that do not correspond to the real anatomy. In SD tractography, the main reasons for false positive reconstructions are the presence of small amplitude spurious FOD components due to noise or the presence of isotropic tissue, and the greater variability due to noise of small but anatomically consistent fiber orientations [Dell'Acqua et al., 2010]. To overcome these problems, we propose to use HMOA thresholds as exclusion criteria for seeding, propagating, and stopping tracking. Here, we apply this idea to a simple deterministic tractography algorithm, although the same approach is also applicable to other algorithms including probabilistic or more complex approaches.

The tractography algorithm can be described by the following steps:

1. For each brain voxel, the orientations of the FOD local maxima are calculated and only those orientations whose amplitude is above the absolute and relative thresholds as described in the previous paragraph are considered as estimates of true fiber orientations.
2. Whole brain tractography is started from all voxels with at least one fiber orientation. For voxels with n fiber orientations, n streamlines are propagated with Eulerian integration and a fixed step size of 0.5 mm [Basser et al., 2000].
3. At each step, a trilinear interpolation of the surrounding orientations is performed. Only those orientations within 45° of the incoming streamline orientation are included in the interpolation. In the presence of multiple orientations that satisfy this condition within the same voxel, the direction of least curvature is chosen. This condition aims to exclude from the interpolation orientations that are more likely to belong to other tracts. The advantage of this step is that only components that are consistent with the current WM orientation are included and unrelated orientations as well as voxels from isotropic tissue without a proper fiber orientation are excluded.
4. Together with the new orientation, the corresponding HMOA along the streamline is interpolated. If the interpolated HMOA value is above the absolute threshold chosen in step (1) the propagation of the streamline is continued and the algorithm is repeated from step (3). The algorithm stops when the HMOA value is below the absolute threshold.

Numerical Simulations

Numerical simulations were performed to assess how changes in the diffusion properties of one or more fibers can affect SD and the recovered HMOA values. A first group of simulations was performed to study the correspondence between the classical diffusion indices, such as FA and MD, and the HMOA for three different signal configurations:

1. A single fiber characterized by a tensor with fixed axial diffusivity ($D_a = 1.7 \times 10^{-3}$ mm^2/s) and increasing radial diffusivity ($D_r = 0 - 1.0 \times 10^{-3}$ mm^2/s).
2. A single fiber described by a model of restricted diffusion based on the van Gelderen model for diffusion inside an impermeable cylinder. Here, this model is used to mimic intra-axonal diffusion and provides a simplified model to simulate white matter anisotropy variations based on microstructural changes of the fiber ($D_{axon} = 1.7 \times 10^{-3}$ mm^2/s and radius increasing from 0 to 20 μm).
3. A crossing configuration with crossing angles ranging from 0° to 90° characterized by two identical fibers described by a diffusion tensor equal to [1.7 0.2 0.2] $\times$ 10^{-3} mm^2/s.

A second group of simulations was then performed to investigate in more detail crossing configurations where the diffusion properties varied in only one of the two fibers, whereas the second fiber remained fixed. Three conditions of four distinct diffusion configurations were simulated for Fiber 1:

1. Changes in radial diffusivity only, corresponding to diffusion tensors equal to [1.7 0.2 0.2], [1.7 0.3 0.3], [1.7 0.4 0.4], [1.7 0.5 0.5] $\times$ 10^{-3} mm^2/s.
2. Changes in axial diffusivity only, corresponding to diffusion tensors equal to [1.7 0.2 0.2], [1.5 0.2 0.2], [1.3 0.2 0.2], [1.1 0.2 0.2] $\times$ 10^{-3} mm^2/s.
3. Changes in the overall anisotropy while keeping the tensor trace of the fiber fixed, corresponding to diffusion tensors equal to [1.7 0.2 0.2], [1.5 0.3 0.3], [1.3 0.4 0.4], [1.1 0.5 0.5] $\times$ 10^{-3} mm^2/s.

The diffusivity of Fiber 2 was kept constant at [1.7 0.2 0.2] $\times$ 10^{-3} mm^2/s. Signals were simulated for three crossing angles (50°, 70°, and 90°), corresponding to totally resolved crossing configurations.

All synthetic data was generated to match our in vivo HARDI protocol, corresponding to 60 uniformly distributed diffusion gradient directions [Cook et al., 2007] and a b-value of 3000 s/mm^2. For the restricted diffusion case, diffusion gradients were also chosen to match the

parameters used on our clinical scanner ($\Delta = 40$ ms, $\delta = 30$ ms, $G = 40$ mT/m very close to a b-value of 3000 s/mm^2). For each configuration, 500 trials were generated adding Rician noise corresponding to a signal to noise ratio (SNR) equal to 20 for the signal measured with no diffusion weighting.

SD was performed using the damped version of the Richardson Lucy algorithm with parameters as described in [Dell'Acqua et al., 2010]. For the first group of simulations, a fixed fiber response corresponding to a shape factor of $\alpha = 1.5 \times 10^{-3}$ mm^2/s was chosen. For the second group of simulations, to also assess the effect of different fiber responses on the estimated HMOA indices, three different fiber responses corresponding to shape factors of $\alpha = 1.0$, 1.5, and 2.0×10^{-3} mm^2/s were applied.

In Vivo MRI Data

MRI acquisition

Diffusion MRI data was acquired from 30 healthy normal volunteers using a 3 T GE Signa HDx TwinSpeed system (General Electric, Milwaukee, WI). Data was acquired with the following parameters: voxel size $2.4 \times 2.4 \times 2.4$ mm, matrix $= 128 \times 128$, field of view $= 307 \times 307$ mm, 60 slices, 1 average, TE = 93.4 ms, b-value = 3000 s/mm^2, 60 diffusion-weighted directions and 7 nondiffusion-weighted volumes, using a spin-echo single-shot echo-planar imaging (EPI) sequence with an ASSET factor of 2. Peripheral gating was applied with an effective TR of 20/30 R-R intervals. Quality of EPI data was assessed using an automated analysis technique [Simmons et al., 1999]. The study was approved by the Joint Medical Ethical Committee of the Institute of Psychiatry, King's College London and informed consent was obtained from all subjects.

Processing

Diffusion datasets were corrected for head motion and eddy current distortions by applying an affine registration to a nondiffusion-weighted reference volume as implemented in the FSL software package [Smith et al., 2004]. The estimation of the FOD in each voxel was performed using a SD approach based on the damped version of the Richardson-Lucy algorithm. The damped Richardson-Lucy algorithm provides reliable estimates of the FOD in voxels including mixed contribution of white matter, gray matter, and CSF, thus reducing partial volume effects and spurious fiber orientations. Algorithm parameters were chosen as described in [Dell'Acqua et al., 2010].

NuFO maps with different combinations of absolute and relative thresholds were calculated and compared as described in the previous section. Average NuFO maps of 30 subjects were also calculated. Maps of maximum HMOA were estimated and averaged across the 30 subjects to show how the values of the new index are distributed across the entire brain for the main fiber orientation. To test how HMOA is effective as a threshold to stop tractography in regions of low anisotropy, whole brain tractography was performed as described in the previous section. Dissections of the left Cingulum were performed on three subjects by applying two coronal regions of interest (ROI) at the level of the isthmus and the anterior-mid body of the corpus callosum. No exclusion ROI was applied to avoid masking the effect of HMOA thresholds. As reference, the same tracts were dissected using DTI tractography and the same ROIs. Whole-brain DTI tractography was performed using ExploreDTI [Leemans et al., 2009] with an FA threshold of 0.2, Euler integration with 0.5 mm step size and angle threshold of 45°. All virtual dissections were performed using Trackvis [Wang et al., 2007]. Finally, to show the difference between tract specific measurements based on voxel-based indices like FA and the true tract-specific HMOA index, we also performed the dissection of a portion of the corona radiata, in a region that includes crossing fibers from the corpus callosum, the CST, and the arcuate fascicle (AF). FA and HMOA values were mapped along each tract.

RESULTS

Numerical Simulation

Figure 3 shows how HMOA, FA, and MD vary with (a) radial diffusivity, (b) axonal radius, and (c)crossing angle. HMOA decreases with increasing values of radial diffusivity and axonal radius. A similar pattern was also found for FA, with some differences. For increases in radial diffusivity, the HMOA decrease is faster and follows an exponential-like profile, whereas for increases in axonal radius the HMOA changes begin earlier (i.e., 3 μm) and show a greater rate of decrease compared with FA. In the crossing fiber configuration, for angles of 0–40° (where the fiber crossing is not resolved), HMOA decreases, whereas FA remains almost stationary. For angles >40°, the HMOA profile shows minimal variation, whereas FA shows an increased decay rate which is at its maximum for values between 60° and 80°. This suggests that while HMOA is minimally affected when fiber crossing is resolved as distinct FOD lobes, FA values vary significantly for fiber crossing angles greater than 40° and the crossing angle became a major factor for FA differences. The MD values increase for the increasing radial diffusivity and axonal radius configurations and slightly decrease for the fiber-crossing configuration.

Table I shows the results for the simulation with two crossing fibers in the presence of diffusion changes in only one of the two fibers (Fiber 1). Results include three distinct conditions where changes occur only in the radial diffusivity (top panel), axial diffusivity (middle panel), or in both diffusion components, whereas the trace of the tensor of the fiber is kept fixed (bottom panel). Results are shown for nine configurations of different crossing angles and fiber response functions. As expected, changes in the radial

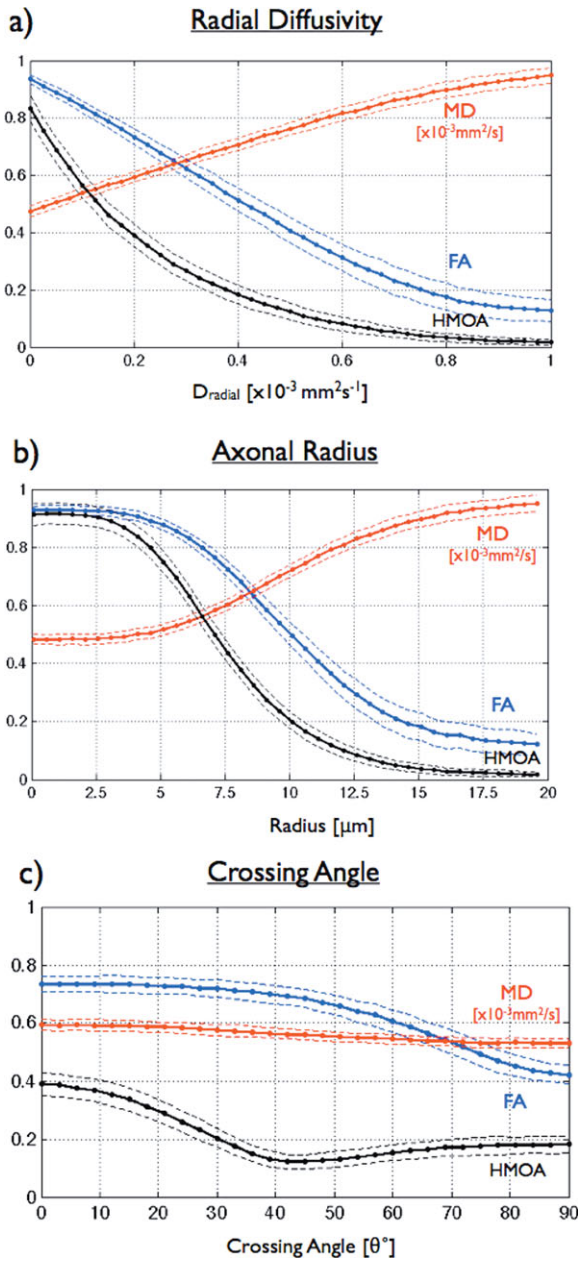

Figure 3.

Simulation results: HMOA, FA, and MD changes in three different fiber configurations. (**a**) A single fiber is simulated with fixed parallel diffusivity and increasing radial diffusivity. (**b**) A single fiber is described with a model of restricted diffusion inside a cylinder and increasing radius. (**c**) A crossing configuration between two identical fibers is shown for increasing crossing angle. In all simulations, the solid line represents the average value over 500 trials and the dotted lines the standard deviation.

diffusivity of Fiber 1 greatly affect the amplitude of the corresponding FOD lobe in all configurations, with more than sixfold variations in some configuration. Similar results are also obtained for changes in axial diffusivity but with smaller variations. Combined changes of axial and radial diffusivity show even larger variations in the value of HMOA index (up to eightfold). The amplitude of Fiber 2 is minimally affected for most of the configurations (variations are around 10% in the worst case) except for configurations with the smallest crossing angle. Here, however, rounded profiles in the FOD lobes also suggest a general decreased angular resolution of the recovered FOD profiles. Figure 4 shows simulation results in the case of combined changes in both axial and radial diffusivity; similar profiles are also obtained for changes only in radial or axial diffusivity. By increasing the shape factor of the fiber response, the angular resolution of the FOD profile increases and changes in the amplitude of Fiber 2 reduce.

When comparing the results of each configuration with the corresponding diffusion tensor, we can observe that diffusion changes in only one of the crossing fibers usually produce small or moderate changes in the overall tensor ellipsoid profiles and their corresponding FA and MD values. Unexpectedly, we also observe that in the 90° crossing configuration, while the anisotropy of Fiber 1 monotonically decreases, FA values show a nonmonotonic inversion. This effect is visible in the conditions of radial diffusivity changes and combined diffusion changes. When changes occur only in axial diffusivity, FA changes are almost negligible and only MD decreases.

In Vivo Results

In this section, we present the in vivo results from healthy subjects where diffusion datasets were processed using the dRL algorithm to create individual FOD maps, NuFO maps, and to perform tractography.

Figure 5a shows a sagittal slice of FOD profiles, which includes fibers of the major association tracts and some lateral projections of the corpus callosum. For each voxel, the absolute amplitude of the FOD is displayed which gives a visual representation of the HMOA variations between different voxels. A direct comparison between the FOD map and a corresponding DT-ellipsoid map shows that for voxels with a single or a major fiber orientation both maps provide similar directional information. However, in regions with crossing fibers where the tensor shows only an average orientation, distinct white matter orientations often merge as a single continuous tract. For example in Figure 5a, this effect is visible between portions of the AF and the inferior frontal occipital fascicle running in the temporal stem.

The HMOA of each FOD lobe also shows smooth changes across adjacent voxels thus describing a continuous representation of the diffusion properties that propagate along the same tract. For example in Figure 5a, smooth changes in HMOA can be observed along the AF, the inferior longitudinal fasciculus, and the tracts of the external capsule, facilitating the identification of the

TABLE I. Simulation results: Diffusion changes in a crossing configuration

		Fiber response						Diffusion tensor	
		$\alpha = 1.0$		$\alpha = 1.5$		$\alpha = 2.0$			
Angle (°)		HMOA fiber 1	HMOA fiber 2	HMOA fiber 1	HMOA fiber 2	HMOA fiber 1	HMOA fiber 2	FA	MD
Radial diffusion changes									
50	1	0.12 ± 0.02	0.12 ± 0.02	0.13 ± 0.03	0.13 ± 0.03	0.14 ± 0.03	0.14 ± 0.04	0.66 ± 0.04	0.55 ± 0.02
	2	0.06 ± 0.02	0.14 ± 0.03	0.08 ± 0.02	0.14 ± 0.03	0.09 ± 0.03	0.15 ± 0.04	0.61 ± 0.04	0.59 ± 0.02
	3	0.03 ± 0.01	0.16 ± 0.03	0.04 ± 0.02	0.15 ± 0.03	0.05 ± 0.03	0.16 ± 0.04	0.57 ± 0.04	0.62 ± 0.02
	4	—	0.17 ± 0.03	0.02 ± 0.01	0.16 ± 0.04	0.03 ± 0.02	0.16 ± 0.04	0.54 ± 0.04	0.65 ± 0.02
70	1	0.17 ± 0.02	0.17 ± 0.02	0.17 ± 0.03	0.17 ± 0.03	0.17 ± 0.04	0.17 ± 0.04	0.53 ± 0.04	0.53 ± 0.02
	2	0.10 ± 0.02	0.18 ± 0.03	0.11 ± 0.03	0.18 ± 0.03	0.11 ± 0.03	0.17 ± 0.04	0.49 ± 0.04	0.57 ± 0.02
	3	0.06 ± 0.02	0.18 ± 0.03	0.07 ± 0.02	0.18 ± 0.04	0.07 ± 0.03	0.17 ± 0.04	0.47 ± 0.04	0.61 ± 0.02
	4	0.03 ± 0.01	0.18 ± 0.03	0.04 ± 0.02	0.18 ± 0.03	0.04 ± 0.02	0.17 ± 0.04	0.47 ± 0.04	0.64 ± 0.02
90	1	0.19 ± 0.02	0.19 ± 0.02	0.18 ± 0.03	0.18 ± 0.03	0.17 ± 0.04	0.17 ± 0.04	0.43 ± 0.03	0.53 ± 0.01
	2	0.12 ± 0.02	0.19 ± 0.03	0.12 ± 0.03	0.18 ± 0.03	0.11 ± 0.03	0.17 ± 0.04	0.40 ± 0.03	0.57 ± 0.02
	3	0.07 ± 0.02	0.19 ± 0.03	0.07 ± 0.03	0.18 ± 0.03	0.07 ± 0.03	0.17 ± 0.04	0.41 ± 0.03	0.61 ± 0.02
	4	0.04 ± 0.02	0.19 ± 0.03	0.04 ± 0.02	0.18 ± 0.03	0.04 ± 0.02	0.17 ± 0.04	0.42 ± 0.04	0.64 ± 0.02
Axial diffusion changes									
50	1	0.12 ± 0.02	0.12 ± 0.02	0.13 ± 0.03	0.13 ± 0.03	0.14 ± 0.04	0.15 ± 0.04	0.66 ± 0.04	0.55 ± 0.02
	2	0.11 ± 0.02	0.12 ± 0.02	0.11 ± 0.03	0.13 ± 0.03	0.12 ± 0.03	0.14 ± 0.04	0.67 ± 0.04	0.54 ± 0.02
	3	0.09 ± 0.02	0.13 ± 0.02	0.09 ± 0.03	0.13 ± 0.03	0.10 ± 0.03	0.14 ± 0.04	0.66 ± 0.04	0.52 ± 0.02
	4	0.07 ± 0.02	0.14 ± 0.03	0.07 ± 0.02	0.14 ± 0.03	0.07 ± 0.03	0.14 ± 0.04	0.66 ± 0.04	0.50 ± 0.02
70	1	0.17 ± 0.02	0.17 ± 0.02	0.17 ± 0.03	0.17 ± 0.03	0.17 ± 0.04	0.17 ± 0.04	0.53 ± 0.04	0.54 ± 0.02
	2	0.16 ± 0.02	0.17 ± 0.02	0.15 ± 0.03	0.17 ± 0.03	0.14 ± 0.04	0.17 ± 0.04	0.53 ± 0.04	0.52 ± 0.01
	3	0.14 ± 0.02	0.16 ± 0.02	0.13 ± 0.03	0.16 ± 0.03	0.12 ± 0.04	0.16 ± 0.04	0.53 ± 0.04	0.51 ± 0.01
	4	0.12 ± 0.02	0.16 ± 0.03	0.10 ± 0.03	0.16 ± 0.03	0.09 ± 0.03	0.15 ± 0.04	0.52 ± 0.04	0.48 ± 0.01
90	1	0.19 ± 0.02	0.19 ± 0.02	0.18 ± 0.03	0.18 ± 0.03	0.17 ± 0.04	0.17 ± 0.04	0.43 ± 0.03	0.53 ± 0.01
	2	0.18 ± 0.02	0.18 ± 0.03	0.16 ± 0.03	0.17 ± 0.03	0.14 ± 0.04	0.16 ± 0.04	0.43 ± 0.03	0.51 ± 0.01
	3	0.16 ± 0.02	0.18 ± 0.02	0.13 ± 0.03	0.17 ± 0.03	0.11 ± 0.04	0.16 ± 0.04	0.42 ± 0.03	0.50 ± 0.01
	4	0.13 ± 0.02	0.17 ± 0.02	0.10 ± 0.03	0.16 ± 0.03	0.08 ± 0.03	0.15 ± 0.04	0.41 ± 0.03	0.48 ± 0.01
Anisotropy changes (fixed trace)									
50	1	0.12 ± 0.02	0.12 ± 0.02	0.13 ± 0.03	0.13 ± 0.03	0.14 ± 0.04	0.14 ± 0.04	0.66 ± 0.04	0.55 ± 0.02
	2	0.06 ± 0.02	0.14 ± 0.03	0.07 ± 0.02	0.14 ± 0.03	0.08 ± 0.03	0.15 ± 0.04	0.61 ± 0.04	0.58 ± 0.02
	3	0.02 ± 0.01	0.16 ± 0.03	0.03 ± 0.02	0.15 ± 0.03	0.04 ± 0.02	0.15 ± 0.04	0.57 ± 0.04	0.60 ± 0.02
	4	—	0.18 ± 0.03	0.01 ± ± 0.01	0.16 ± 0.04	0.02 ± 0.01	0.16 ± 0.04	0.53 ± 0.04	0.61 ± 0.02
70	1	0.17 ± 0.02	0.17 ± 0.02	0.17 ± 0.03	0.17 ± 0.03	0.17 ± 0.04	0.17 ± 0.04	0.54 ± 0.04	0.54 ± 0.02
	2	0.10 ± 0.02	0.18 ± 0.02	0.10 ± 0.03	0.17 ± 0.03	0.09 ± 0.03	0.17 ± 0.04	0.49 ± 0.05	0.56 ± 0.02
	3	0.05 ± 0.02	0.18 ± 0.03	0.05 ± 0.02	0.17 ± 0.03	0.04 ± 0.02	0.16 ± 0.04	0.47 ± 0.04	0.58 ± 0.02
	4	0.02 ± 0.01	0.18 ± 0.03	0.02 ± 0.01	0.17 ± 0.03	0.02 ± 0.02	0.17 ± 0.04	0.46 ± 0.04	0.60 ± 0.02
90	1	0.19 ± 0.02	0.19 ± 0.02	0.18 ± 0.03	0.18 ± 0.03	0.17 ± 0.04	0.17 ± 0.04	0.43 ± 0.03	0.53 ± 0.02
	2	0.11 ± 0.02	0.19 ± 0.03	0.10 ± 0.03	0.18 ± 0.03	0.09 ± 0.03	0.17 ± 0.04	0.40 ± 0.03	0.56 ± 0.02
	3	0.06 ± 0.02	0.18 ± 0.03	0.05 ± 0.02	0.17 ± 0.03	0.04 ± 0.02	0.16 ± 0.04	0.41 ± 0.04	0.58 ± 0.02
	4	0.02 ± 0.01	0.18 ± 0.03	0.02 ± 0.02	0.17 ± 0.03	0.02 ± 0.02	0.16 ± 0.04	0.43 ± 0.04	0.60 ± 0.02

Three separate conditions of diffusion changes are simulated for fiber 1. Top table, changes only in radial diffusivity (fiber 1 FA = 0.87, 0.80, 0.73, 0.65 and MD = 0.70, 0.77, 0.83, 0.90 × 10^{-3} mm^2/s); Middle table, changes only in axial diffusivity (fiber 1 FA = 0.87, 0.85, 0.83, 0.79 and MD = 0.70, 0.63, 0.57, 0.50 × 10^{-3} mm^2/s); Bottom table, changes in overall anisotropy keeping the same tensor trace (fiber 1 FA = 0.87, 0.77, 0.63, 0.46 and MD = 0.70 × 10^{-3} mm^2/s). Fiber 2 is always kept fixed (FA = 0.87 and MD = 0.70 × 10^{-3} mm^2/s). Results are shown for three different crossing angles (50°, 70°, 90°). The four values in each cell of the table, from top to bottom, are the results corresponding to the four diffusion changes applied to fiber 1. From left to right the first three pairs of columns show HMOA values of the two fiber orientations for the three chosen fiber response functions (α = 1.0, 1.5, 2.0 × 10^{-3} mm^2/s). The last column on the right shows the equivalent FA and MD values.

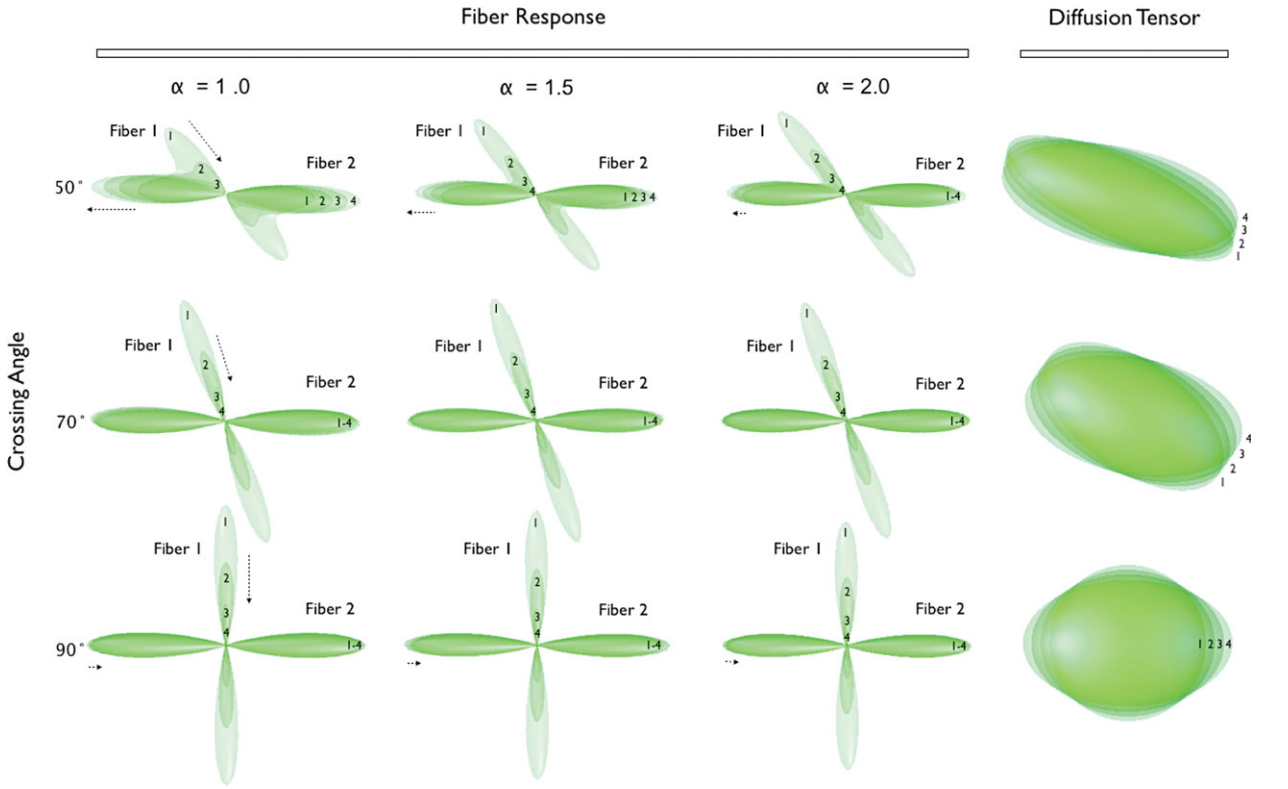

Figure 4.

Simulation results: Diffusion changes in a crossing configuration. This figure shows, as an example, average FOD profiles and tensor ellipsoids for changes in the anisotropy of Fiber 1, whereas keeping Fiber 2 fixed (Fiber 1 FA = 0.87, 0.77, 0.63, 0.46 and MD = 0.70 × 10^{-3} mm^2/s, Fiber 2 FA = 0.87 and MD = 0.70 × 10^{-3} mm^2/s). On the left, FOD profiles are overlaid to show how anisotropy changes in Fiber 1 affects the recovered FOD lobes. Three crossing angles (50°, 70°, and 90°) and three applied fiber response function (α = 1.0, 1.5, 2.0 × 10^{-3} mm^2/s) are shown. On the right, the corresponding diffusion ellipsoids show the same changes as described by the diffusion tensor model. Similar results are obtained also with changes in radial or axial diffusivity only.

anatomy of each tract. In Figure 5b, three voxels, corresponding to three locations with the same FA (i.e., same gray level) are highlighted to show how, although the anisotropy of the voxel is the same, they are instead characterized by different HMOA values thus revealing a deeper complexity of microstructural architecture.

NuFO maps and maximum HMOA maps

NuFO maps allow the visualization of the number of distinct fiber orientations in each voxel, which is a useful index of local white matter complexity. Figure 6a shows the application of the two-threshold approach for the estimation of the NuFO maps. The human brain shows a high degree of local complexity (number of fibers ≥ 2) in many white matter regions. In Figure 6b, multiple fiber orientations are visible in the corona radiata and in periventricular voxels. Regions that have only one fiber population are the corpus callosum, corticospinal tract, and white matter adjacent to the cortex. The appearance of NuFO maps varies according to the applied thresholds, whereas the relative distribution of number of fibers appears to be consistent with small variations across different subjects (Table II). For higher absolute thresholds, the number of voxels characterized by multiple orientations decreases as expected, whereas the percentage of single orientation voxels increases. From these results, it can be observed that the choice of the absolute threshold is also dependent on the quality of the data (e.g., SNR) and the regularization capabilities of the deconvolution algorithm to remove spurious components. Therefore, rather than defining a single optimal threshold, different thresholds can be applied to identify either the most representative FOD components or specific ranges of HMOA values. A further but minimal reduction of multiple orientations and increase of single fiber configuration is obtained with increasing relative threshold, which results in the reduction of spurious components in regions with high HMOA components (e.g., body of the corpus callosum).

Another advantage of the NuFO maps is the additional anatomical information that is provided compared with

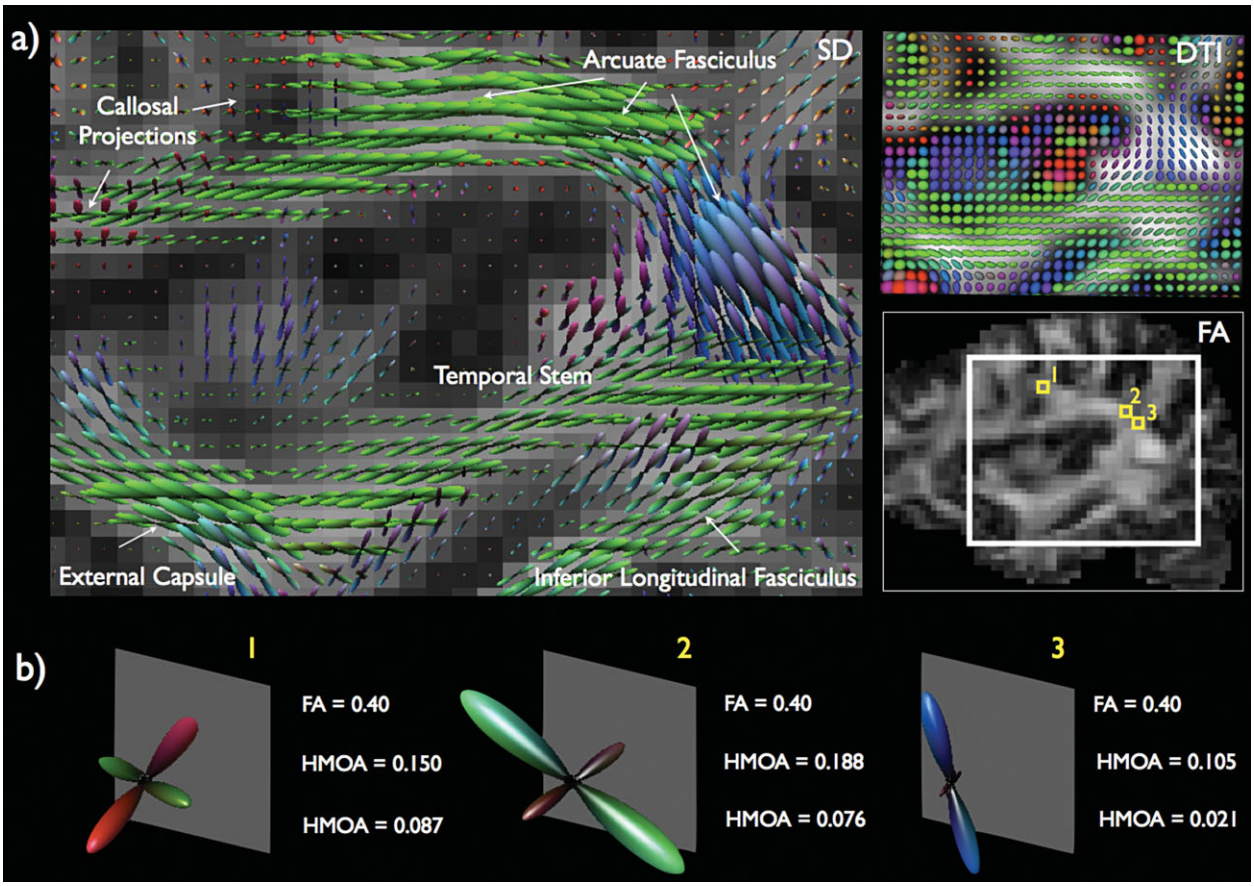

Figure 5.

In vivo results: Absolute FOD profiles. (**a**) Absolute FOD profiles from a sagittal slice, which includes fibers of the major association tracts and the corpus callosum, are shown on the left. This image gives a general overview of HMOA distribution in a large brain region and along different tracts. On the right, the same region is shown using a diffusion tensor ellipsoidal visualization. (**b**) Three voxels selected with the same FA value (yellow squares) show the corresponding HMOA values along the recovered fiber orientations.

FA maps. Figure 7, on the left, shows the average NuFO maps from 30 subjects with an absolute threshold of 4 A_{iso} and a relative threshold of 10%. In these maps, the CST is visible on multiple consecutive slices as an area containing voxels with a single orientation (red arrow), which is not visible in the corresponding FA maps (Fig. 7, centre). Regions with three or more orientations (blue arrows) containing crossing fibers from the corona radiata (projection), corpus callosum (commissural), and superior longitudinal fasciculus (associative) are visible as linear bands bilaterally on the NuFO maps. These areas incorrectly correspond to regions of apparent low anisotropy in the FA maps.

Additionally, Figure 7, on the right, also shows the average map of maximum HMOA in each brain voxel. Although qualitatively similar to classical FA maps, this image provides, for each voxel, quantitative information only about the major white matter component without the contamination of partial volume effects from other fiber orientations. For example in Figure 7, high HMOA values differentiate the AF (green arrow) bilaterally from surrounding brain regions suggesting a different white matter organization along this tract not visible in the FA map. The HMOA index also exhibits smooth changes along white matter tracts confirming that its value is consistent and can be compared across voxels and slices as normally done for FA.

Tractography results

Figure 8 shows the tractography reconstruction of the left Cingulum for three subjects as an example of using HMOA values as a threshold to stop tractography and reduce false positive reconstructions. In these reconstructions, a two-region approach is used to select all the streamlines passing through two coronal ROI placed over

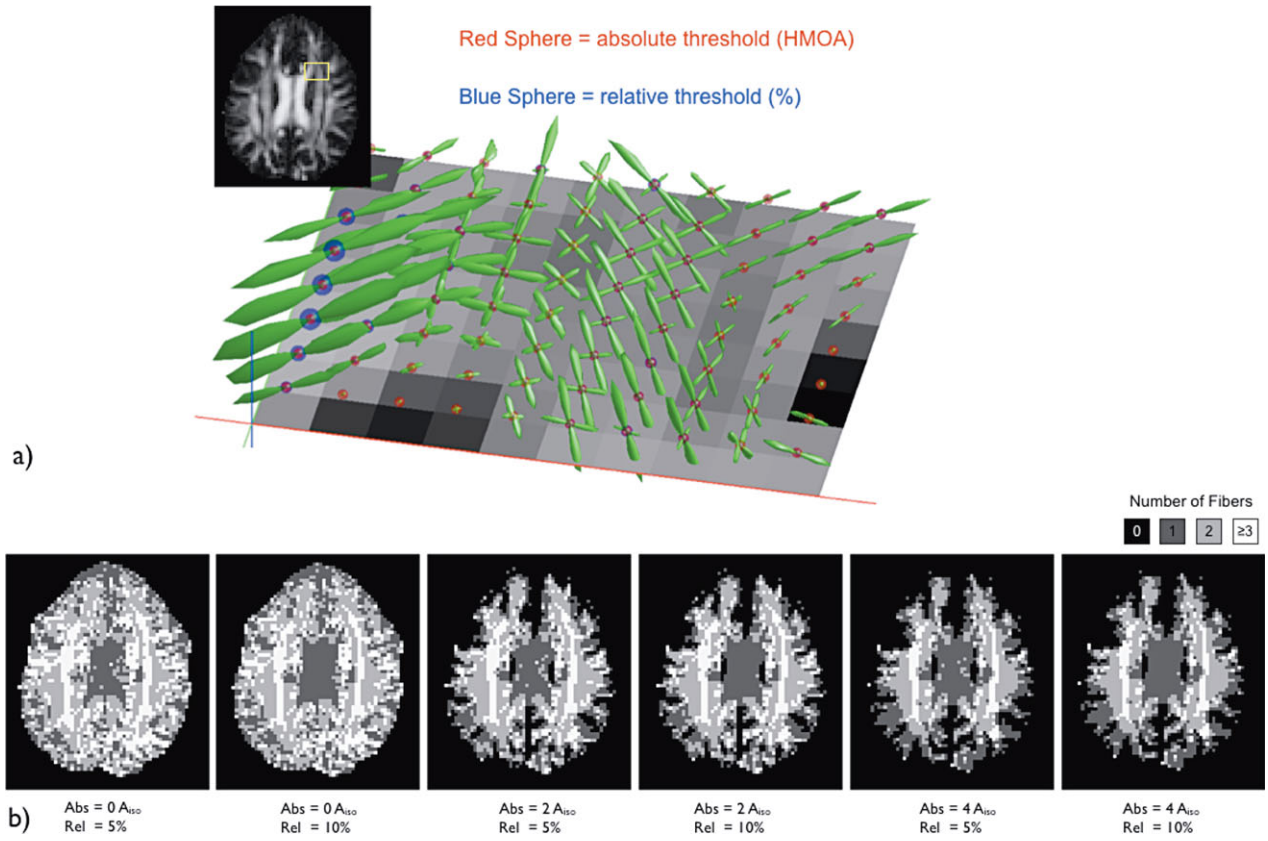

Figure 6.

In vivo results: NuFO maps. (**a**) Visualization of the absolute (red) and relative (blue) thresholds as spherical profiles superimposed on FOD profiles in a selected brain region; (**b**) NuFO maps obtained on a single subject for different values of absolute and relative threshold.

TABLE II. Number of fiber orientations over 30 subjects (%)

	Abs = 0 (HMOA = 0)		Abs = 2 A_{iso} (HMOA = 0.006)		Abs = 4 A_{iso} (HMOA = 0.012)	
Fibers	Rel. = 5%	Rel. = 10%	Rel. = 5%	Rel. = 10%	Rel. = 5%	Rel. = 10%
≥3	32.9 ± 2.2	29.6 ± 2.1	23.6 ± 2.0	22.7 ± 1.9	11.8 ± 1.0	11.7 ± 1.0
2	42.7 ± 1.1	42.7 ± 1.0	41.3 ± 0.9	40.5 ± 0.9	37.2 ± 1.3	36.8 ± 1.3
1	24.4 ± 1.9	27.7 ± 1.9	35.1 ± 2.2	36.8 ± 2.1	51.0 ± 2.1	51.4 ± 2.1

In vivo results: NuFO maps. Distribution of the number of distinct fiber orientations for different absolute and relative threshold levels applied over 30 healthy subjects.

the left Cingulum at the level of the isthmus and anterior-midbody of the corpus callosum. No exclusion ROIs were applied to remove spurious streamlines to show only the effect of HMOA in stopping tractography. By increasing the HMOA threshold from 0.006 to 0.012, most of the false positive reconstructions decrease. By further increasing the threshold to 0.018, other false positives disappear and only components of the Cingulum with higher HMOA are preserved. As verified for the NuFO maps, the results here are also consistent across subjects suggesting that the HMOA can be used reliably as a threshold across subjects. As a comparison, DTI tractography reconstructions of the Cingulum obtained with the same ROI are also shown on the right side of Figure 8. Incomplete reconstructions of the most posterior part of the Cingulum are visible for two of the three subjects.

Figure 9 shows the values of FA and HMOA mapped onto tractography reconstructions of crossing fiber tracts. In white matter regions with only one fiber component, such as the body of the corpus callosum, high values of

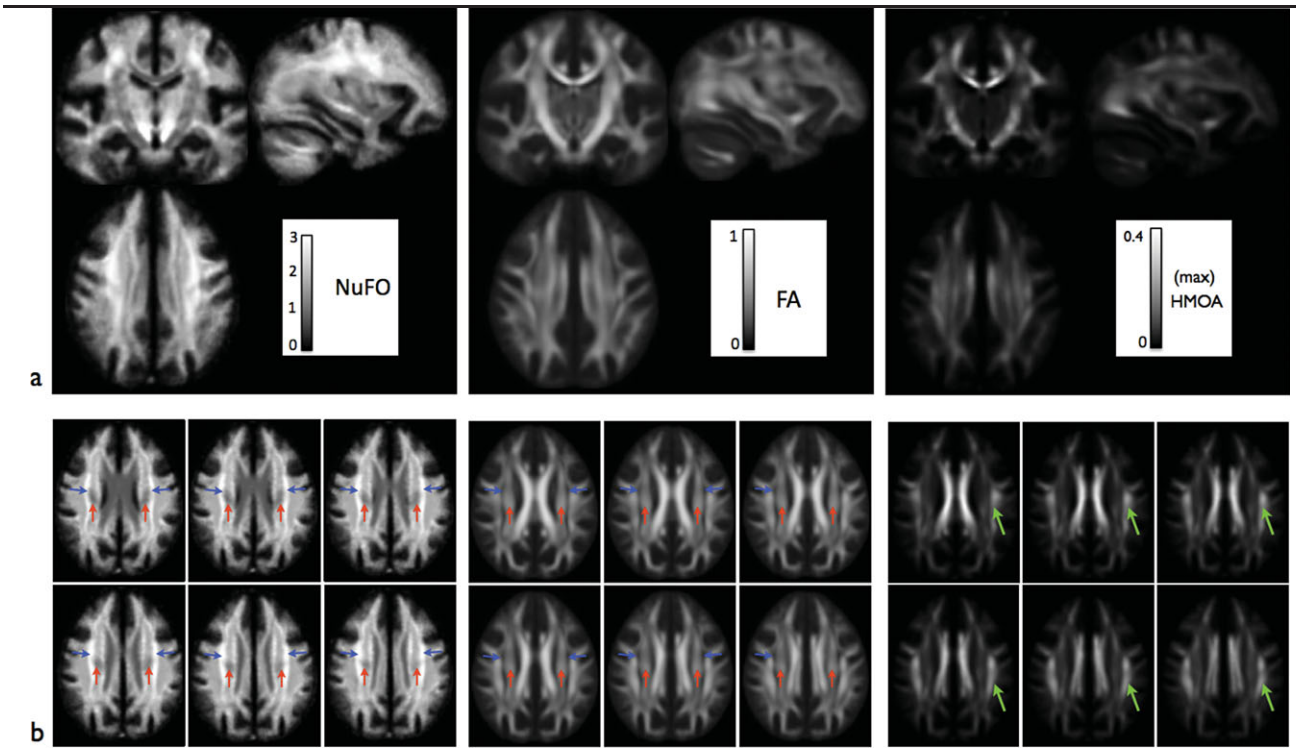

Figure 7.

In vivo results: Average NuFO map and maximum HMOA map from 30 healthy subjects compared with the corresponding average FA map. (**a**) Three orthogonal views show brain regions with different degrees of white matter complexity (left), FA values (centre), and maximum HMOA (right); (**b**) on the left, six consecutive slices show the consistency of the results for regions with one, two, or more than two distinct fiber orientations. Red arrows indicate the central portion of the corticospinal tract as a region with a single fiber orientation. Blue arrows indicate a bilateral band of high white matter complexity with three fiber orientations inside the corona radiata that corresponds to a region of low anisotropy in the FA map (centre). On the right, green arrows indicate a region of high HMOA values corresponding to the arcuate fascicle.

FA correspond to high values of HMOA. In the presence of two or more crossing fibers, FA provides an average, voxel-specific, description of the microstructural organization, which is equally assigned to each fiber component. Conversely, HMOA is a tract-specific index, which can be mapped onto distinct white matter orientations within the same voxel. This allows characterization of the microstructural properties of each fiber component along the same tract and across different voxels. Figure 9 shows two examples of fiber crossing where the advantage of using HMOA to map the microstructural properties of each crossing tract is evident. In the first example, where the fibers of the corpus callosum cross with the central portion of the arcuate fasciculus, both tracts show a reduction in FA, whereas the HMOA values show high HMOA components of the AF crossing with low HMOA callosal tracts (Fig. 9a). In the second example, where the fibers of the CST cross with the most medial fibers of the arcuate fasciculus, both sets of fibers show high levels of FA, whereas high HMOA values are evident only for the fibers of the CST (Fig. 9b). These results show how indices based on the average properties of the voxel may not characterize entirely properties that are specific of each white matter tract, whereas tract specific indices like HMOA can separate diffusion properties of different fiber bundles.

DISCUSSION

In this study, we investigated the use of novel SD derived indices for the quantification of white matter properties in regions with complex microstructural organization. The development of these indices provides a possible solution to two of the main limitations of SD approaches, namely the lack of well-established quantitative measures to apply to normal and clinical populations and the need for a priori knowledge of the fiber response function to apply to the convolution model [Tournier et al., 2004].

In this study, we first observed that changes in the fiber signal profile, either described with a Gaussian or restricted diffusion model, can be reduced to changes in a scaling factor and in a shape factor of the signal fiber profile. Although scale differences translate directly to scaling

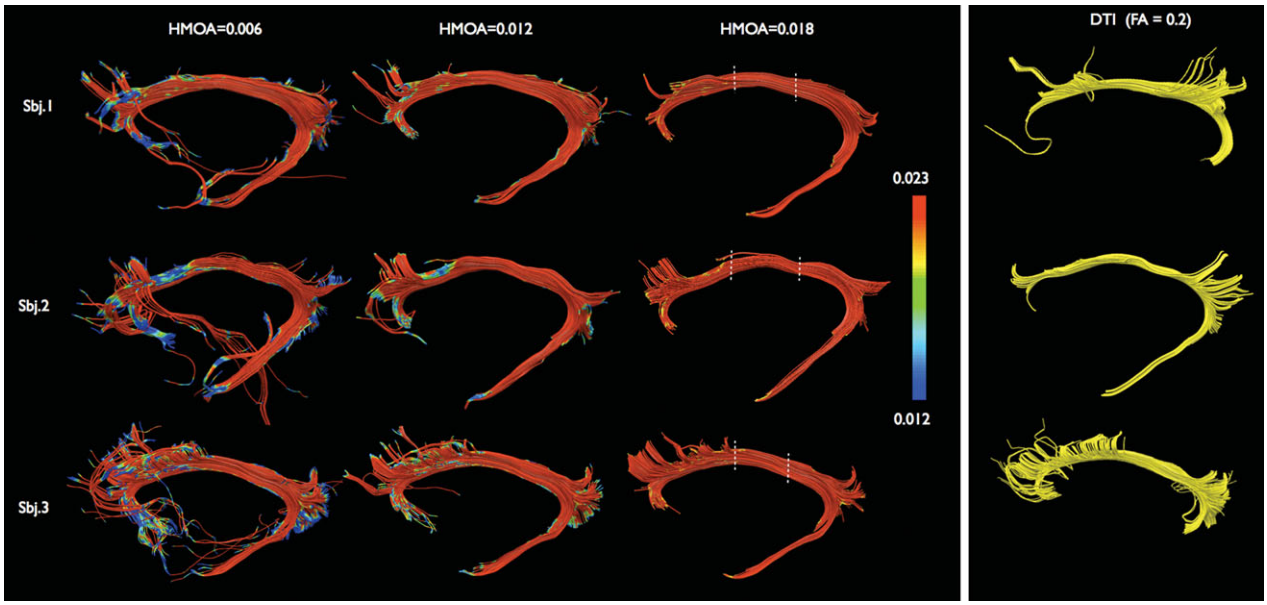

Figure 8.

In vivo results: Tractography reconstruction of the left Cingulum. From left to right, tractography reconstructions are shown with increasing HMOA thresholds for three subjects. To better visualize HMOA differences, HMOA values are mapped along the tracts. The location of the two coronal ROIs used to dissect the tract are shown as white dotted lined on the third column. As a comparison, DTI tractography reconstructions of the Cingulum obtained with the same regions of interest are also shown on the right. No exclusion ROIs were used to remove false positive reconstructions.

of the amplitude of the corresponding FOD lobe, differences in the shape factor modulate a residual blurring that reflects the incomplete deconvolution of the FOD lobe. In agreement with previous studies [Anderson, 2005; Dell'Acqua et al., 2007; Tournier et al., 2004], we found that differences between the measured fiber signal and the chosen fiber response function are always reflected by the SD algorithm as differences in the absolute amplitudes of recovered FOD lobe. Changes in the diffusion signals that occur along all HARDI directions are concentrated and amplified along the specific FOD lobe. This makes the amplitude of each FOD lobe a sensitive index able to detect biological changes that are not "visible" on conventional DTI and that are, at the same time, specific for single fiber orientations. In this study, we formalized the idea originally presented in [Dell'Acqua et al., 2010] to use the amplitude of each FOD lobe as an index of apparent fiber density. A recent paper from [Raffelt et al., in press] following this idea has also proposed the use of the apparent fiber density to perform voxel-based group comparison studies. Here, in this new study, we expanded this concept and demonstrated that the HMOA index provides a compact measure that incorporates information not only about the density of different fiber orientations (expressed as the fiber volume fraction) but also about their diffusion properties including the radial diffusion hindrance and the anisotropy of each fiber orientation. The HMOA is an absolute index that, unlike other HARDI methods that require a local normalization for each voxel, it can be used to directly compare differences across brain regions and between subjects.

In our study, simulation results on a range of anisotropy configurations have shown that changes in either fiber diffusivities or microstructure properties like "axonal" diameters can be better detected by HMOA than by classical FA and MD indices. HMOA shows rapid decays and gives a larger dynamic range to characterize the fiber characteristics. Our simulations with realistic noise levels show that true fiber orientations can be consistently detected down to an HMOA of $\sim$0.01, whereas a single fiber orientation FOD may reach HMOA values of 0.4 or higher in the most anisotropic voxels of the brain. Simulations also confirmed that this index is theoretically able to detect small microstructural changes before they become visible in FA or MD. Changes in axonal radius were visible for fiber radius greater than 3 μm, whereas a clear decrease in FA was visible only after 5 μm. This index may, therefore, be suitable to study axonal changes during white matter maturation or degeneration. Similarly, HMOA was able to detect changes when fiber crossings were not resolved. In these configurations, we observed a rapid decrease of HMOA suggesting that although distinct orientations are not resolved, different degrees of fiber dispersion can be detected by the single recovered FOD lobe. Although this result should be considered in part as a limitation of the use of HMOA to quantify tract specific properties, it

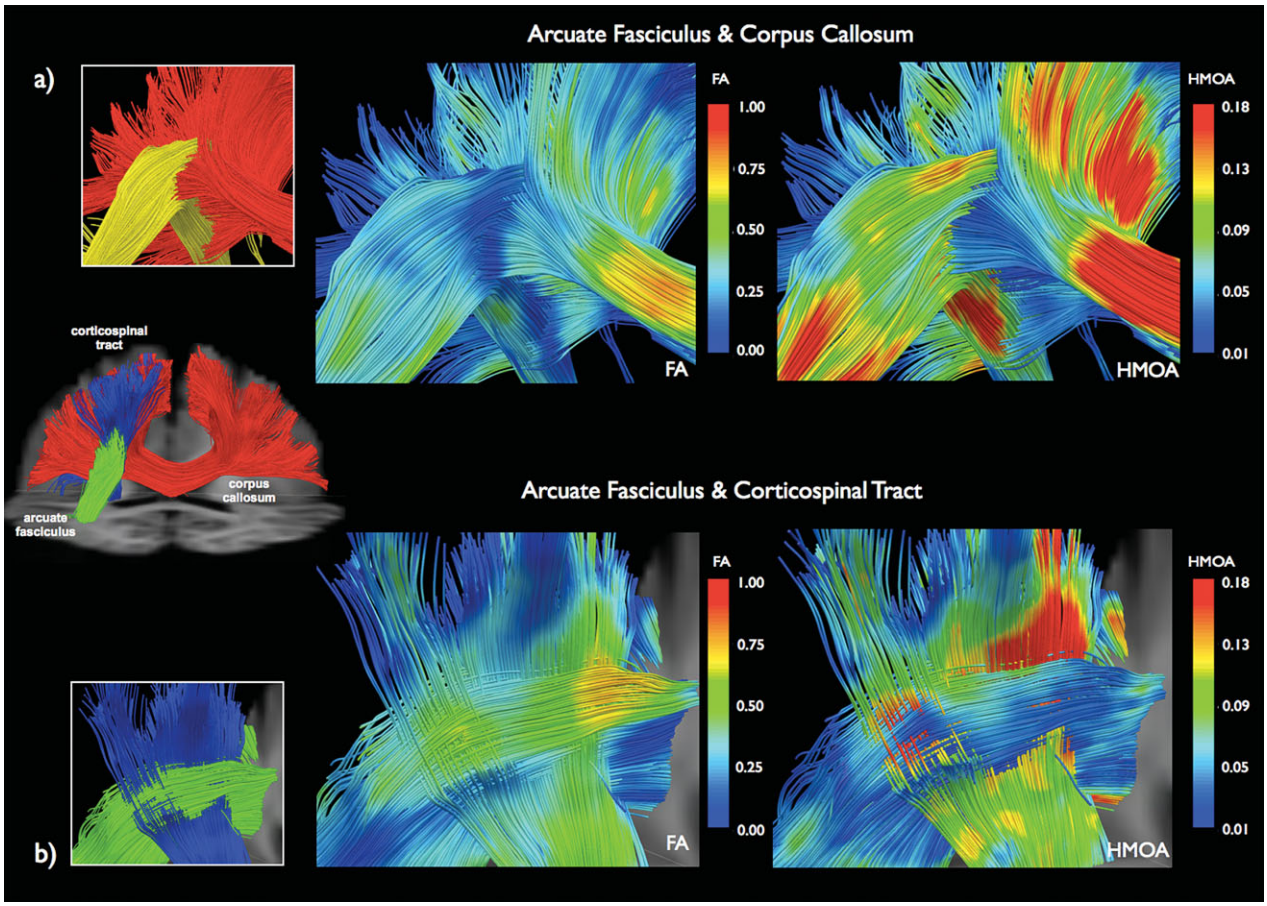

Figure 9.

In vivo results: Mapping FA (left) and HMOA (right) along white matter tracts in the presence of crossing fibers. (**a**) Crossing between a lateral portion of arcuate fascicle and the lateral projections of the corpus callosum. (**b**) Crossing between the cortical spinal tract and a more medial portion of the arcuate fascicle. In both cases, FA values provide an average description of the anisotropic properties of the selected brain region, whereas HMOA shows distinct characteristics for the different white matter tracts.

should also be noted that SD approaches do not fit fiber orientations as a discrete number but as a continuous distribution of the possible orientation. When multiple fiber orientations are not resolved, or a fanning fiber configuration is present, the corresponding FOD lobe correctly describes the average orientation of this group of fibers. Equally here, the HMOA provides an average description of the diffusion properties of the corresponding FOD lobe. Future work may improve the characterization of fiber dispersion by studying not only the amplitude of the recovered HMOA but also fitting and characterizing the shape of the recovered FOD lobe.

For increasing crossing angles, the HMOA decreases until the two fibers are completely resolved. Then, for further increases, the two distinct HMOA values appear less affected by the crossing angle and became more sensitive only to fiber specific changes. In the presence of diffusion changes in a fiber crossing with a second fiber with fixed diffusion characteristics, we observed large variations in HMOA (more than eightfold) along the direction of the FOD lobe of the first fiber. In comparison, voxel-based indices like FA and MD demonstrate only minor variations and in some configurations for a constant decrease in the anisotropy of the first fiber we observed a nonmonotonic behavior in the measured FA (a decrease followed by a subsequent increase in FA). This result confirms previous findings where DTI measurements performed in complex white matter configurations may sometimes lead to results that are difficult to interpret [Wheeler-Kingshott and Cercignani, 2009].

Although, in these simulations, most changes were observed along the corresponding fiber orientation, minor changes were also observed along the second fiber orientation. This effect can be described as a sort of residual

"crosstalk" effect between the fiber orientations that remains even when distinct FOD lobes appear resolved. This effect should be considered a limitation of HMOA estimation, which we believe is mainly due to the intrinsic blurring of the FOD lobes that are not recovered as ideal impulse functions. Our simulations suggest that the magnitude of this "crosstalk" effect depends on the actual crossing angle and on the choice of the fiber response functions, with smaller changes occurring with sharper fiber responses.

It has been previously shown that sharper fiber response (i.e., higher α) allows angular resolution to be increased by resolving small crossing angles [Dell'Acqua et al., 2007]. Here, we observed that the increased angular resolution using a sharper fiber response not only reduces the crosstalk effect for smaller angles but also makes the effect of the crossing less evident on HMOA for larger angles.

On the contrary, by applying fiber responses with smaller α, we observed that due to the larger profile of the fiber response compared with the true signal, each FOD lobe is more likely to include signal contributions from other fiber orientations. Here, small fiber components can be penalized or not resolved if these are close to other large FOD components. In our simulation, Figure 4 shows that with $\alpha = 1.0$ and a crossing configuration of 50°, the smallest fiber component was not resolved. Increasing α in the fiber response allows this component to be resolved. Therefore, higher α seems to provide a better angular resolution, decreased crosstalk effects and also potentially may allow detection of more fiber components that are not resolved at lower α. Our previous study, however, also shows that by increasing α the FOD estimation becomes more sensitive to noise [Dell'Acqua et al., 2007]. Although further studies are required to identify the optimal fiber response function, we think that the choice of fiber response function should be based on a trade off between accuracy of the HMOA measurement and noise stability of the FOD estimation. This removes the need for exact knowledge of the fiber response function, as ideally one would expect to use higher α in high SNR datasets where it is possible to achieve higher angular resolutions and better quantification.

The HMOA represents a first step toward advanced quantitative measures derived from SD. As already highlighted, fitting the shape of the recovered FOD lobes may allow the extraction of more information about white matter organization and, in theory, this may also help to reduce crosstalk effects between FOD lobes. Moreover, because HMOA provides tract specific information, the use of information derived from tractography reconstructions along the entire tract length may also help to better characterize fiber characteristics that are common along the tract or that extend beyond the size of a single voxel.

Previous attempts at using SD for quantifying white matter properties were proposed by Anderson [2005] where, by imposing constraints on the overall voxel tensor trace and assuming common radial diffusivity inside each voxel, it was possible to deconvolve multiple fiber fractions. When compared with this method, our approach has the advantage of not requiring any assumption of the diffusion properties of the fibers and, by measuring a more general HMOA index instead of fitting a specific parameter such as volume fractions, is not sensitive to fitting errors when diffusion properties of the fiber do not match with the fiber response function.

In this study, we also proposed possible applications of the HMOA index. Although this index provides information about the diffusion properties along each white matter orientation, a first direct application could be the use of maximum HMOA maps to investigate white matter changes in case–control group studies. Although qualitatively similar to other anisotropy maps (e.g., FA, GFA, etc.), this map provides only information, in each voxel, about the major fiber orientation without contamination due to partial volume effects from other fiber orientations. From the simulation results, we expect that these maps, combined with tract-based spatial statistics [Smith et al., 2006] analysis or similar approaches, will become a useful and sensitive tool to study white matter in different neurological and psychiatric disorder and allow the detection of changes that may not be possible with conventional diffusion indices.

Finally, the HMOA index can also be used to improve the estimation of other SD-based indices such as the NuFO maps or to improve tractography reconstructions as well as to allow more accurate tract specific quantifications.

NuFO maps

NuFO maps provide a general voxel-based description of white matter complexity according to the number of distinct fiber orientations, which have several potential applications. When compared with color-coded or anisotropy maps, NuFO maps allow regions with low local fiber complexity containing one single orientation (e.g., corticospinal tract) and regions with higher local fiber complexity containing crossing fiber tracts to be distinguished. A close inspection of the NuFO maps (Figs. 6 and 7) reveals a linear band of high fiber complexity (three or more distinct tracts) in-between the central portion of the corona radiata, which represents a transition region between medial projection fibers and lateral association tracts. NuFO maps also appear to be highly consistent across individuals and could therefore represent a sensitive tool to map variations of white matter complexity in healthy populations such as age-related changes or pathology.

Our findings show that the use of an absolute HMOA threshold improves NuFO maps by restricting the estimation of the number of fibers to voxels containing only white matter without requiring an a priori white matter mask. Furthermore, for higher HMOA thresholds, the number of fibers reduces and the distribution of the number of orientations shifts to lower values. Higher HMOA

thresholds allows selective enhancement of only the more representative FOD components by removing small lobes that are more likely to be spurious components or fiber orientations that contribute minimally to the voxel signal. The choice of optimal thresholds is, therefore, based not only on anatomical considerations but also on a number of external factors such as the quality of datasets (e.g., low SNR data requires a higher threshold to exclude more false positives) and the deconvolution algorithm (different regularization approaches may reject noise spikes in different ways). Finally, although NuFO maps provide more information about white matter complexity, it is important to note that they do not yet describe the full microstructural organization of different white matter tracts as a single orientation within a voxel may still describe parallel but distinct tracts or unresolved fanning of multiple white tracts. In regions close to isotropic tissue, partial volume effect also reduces the signal from white matter. Therefore, in such regions, only the main components are detectable, whereas smaller components cannot be separated from noise effects.

Tractography

In this study, we used HMOA for the first time to reconstruct white matter pathways using SD tractography. Our findings show that SD has the advantage over classical DTI tractography of allowing tracking through regions with multiple fibers crossing. This allows the reduction of false negative reconstructions that are usually observed with classical DTI tractography. However, one of the limitations of multiple fiber orientation algorithms is the generation of more false positives. Our findings suggest that false positive reconstructions can be effectively reduced using SD tractography, by applying an HMOA threshold as a stopping criterion for the tracking algorithm. However, future tractography studies are needed to optimize HMOA threshold values and assess the validity of SD tractography in well-known anatomical structures.

In this study, we have shown that, by mapping HMOA on tractography reconstructions, we can also visualize and extract additional information about individual white matter tracts in regions with crossing fibers. Tract-specific measurements have been previously used to quantify variations in healthy brains and in brain disorders using indices derived from diffusion imaging or other MR techniques such as T_1, T_2 values, or myelination fraction [Deoni et al., 2008]. However, interpretation of the results is often not straightforward because these measurements refer to information based on average voxel characteristics and do not discriminate between different fiber bundles. On the contrary, HMOA represents a true tract-specific index and we have shown that low HMOA tracts can be separated from high HMOA tracts inside the same voxel or brain region (e.g., Figure 9, crossing between the AF and CST). HMOA also appears to change smoothly along tracts, suggesting that the variation of this index may better describe the underlying microstructural properties of the specific bundles. Therefore, this index could represent a significant advancement for the study of white matter where changes may involve only specific tracts and leave intact other healthy crossing tracts in the same region. Finally, in the future, this index could potentially also help to develop new tractography methods that are able not only to address the problem of crossing fibers but, by following "tract similarities", also to discriminate between crossing, bending, or kissing configurations.

CONCLUSIONS

In this article, we studied novel indices derived from SD to characterize white matter changes and organization. The HMOA is a tract-specific and sensitive index that can detect small changes in the microstructural properties along single white matter tracts, which may not be detectable with conventional DTI. In this study we observed promising results from data simulated over a range of diffusion configurations that we expect to occur during brain development, aging, and pathological disorders. Applied to in vivo data on healthy subjects, HMOA, NuFO maps, and tractography reconstructions allowed improved characterization of white matter complexity suggesting that these indices can provide a new set of useful tools to better quantify white matter changes. However, to verify the validity of HMOA as a clinical index, further studies on clinical populations are required.

REFERENCES

Aboitiz F, Lòpez J, Montiel J (2003): Long distance communication in the human brain: Timing constraints for inter-hemispheric synchrony and the origin of brain lateralization. Biol Res 36:89–99.

Alexander DC (2005): Maximum entropy spherical deconvolution for diffusion MRI. Image Process Med Imaging 19:76–87.

Alexander DC, Hubbard PL, Hall MG, Moore EA, Ptito M, Parker GJM, Dyrby TB (2010): Orientationally invariant indices of axon diameter and density from diffusion MRI. NeuroImage 52:1374–1389.

Anderson AW (2005): Measurement of fiber orientation distributions using high angular resolution diffusion imaging. Magn Reson Med 54:1194–1206.

Assaf Y, Basser PJ (2005): Composite hindered and restricted model of diffusion (CHARMED) MR imaging of the human brain. NeuroImage 27:48–58.

Assaf Y, Freidlin RZ, Rohde GK, Basser PJ (2004): New modeling and experimental framework to characterize hindered and restricted water diffusion in brain white matter. Magn Reson Med 52:965–978.

Assaf Y, Blumenfeld-Katzir T, Yovel Y, Basser PJ (2008): AxCaliber: A method for measuring axon diameter distribution from diffusion MRI. Magn Reson Med 59:1347–1354.

Barazany D, Basser PJ, Assaf Y (2009): In vivo measurement of axon diameter distribution in the corpus callosum of rat brain. Brain 132 (Part 5):1210–1220.

Basser PJ, Mattiello J, LeBihan D (1994): Estimation of the effective self-diffusion tensor from the NMR spin echo. J Magn Reson B 103:247–254.

Basser PJ, Pajevic S, Pierpaoli C, Duda J, Aldroubi A (2000): In vivo fiber tractography using DT-MRI data. Magn Reson Med 44:625–632.

Beaulieu C (2002): The basis of anisotropic water diffusion in the nervous system—A technical review. NMR Biomed 15:435–455.

Behrens TE, Berg HJ, Jbabdi S, Rushworth MF, Woolrich MW (2007): Probabilistic diffusion tractography with multiple fibre orientations: What can we gain? NeuroImage 34:144–155.

Berman JI, Chung S, Mukherjee P, Hess CP, Han ET, Henry RG (2008): Probabilistic streamline q-ball tractography using the residual bootstrap. NeuroImage 39:215–222.

Cook PA, Symms M, Boulby PA, Alexander DC (2007): Optimal acquisition orders of diffusion-weighted MRI measurements. J Magn Reson Imaging 25:1051–1058.

Dell'Acqua F, Rizzo G, Scifo P, Clarke RA, Scotti G, Fazio F (2007): A model-based deconvolution approach to solve fiber crossing in diffusion-weighted MR imaging. IEEE Trans Biomed Eng 54:462–472.

Dell'Acqua F, Scifo P, Catani M, Scotti G, Fazio F (2008): Combining spherical deconvolution with streamline tractography: Preliminary results. In: Proceedings 16th Scientific Meeting, International Society of Magnetic Resonance in Medicine, Toronto, Canada.

Dell'Acqua F, Coward J, Simmons A, Murphy D, Williams S, Catani M (2009): Mapping crossing fibres of the human brain with spherical deconvolution: Towards an atlas for clinico-anatomical correlation studies. In: Proceedings 17th Scientific Meeting, International Society for Magnetic Resonance in Medicine, Honolulu, USA.

Dell'Acqua F, Scifo P, Rizzo G, Catani M, Simmons A, Scotti G, Fazio F (2010): A modified damped Richardson-Lucy algorithm to reduce isotropic background effects in spherical deconvolution. NeuroImage 49:1446–1458.

Deoni SCL, Rutt BK, Arun T, Pierpaoli C, Jones DK (2008): Gleaning multicomponent T_1 and T_2 information from steady-state imaging data. Magn Reson Med 60:1372–1387.

Dubois J, Dehaene-Lambertz G, Perrin M, Mangin J, Cointepas Y, Duchesnay E, Le Bihan D, Hertz-Pannier L (2008): Asynchrony of the early maturation of white matter bundles in healthy infants: Quantitative landmarks revealed noninvasively by diffusion tensor imaging. Hum Brain Mapp 29:14–27.

Grebenkov D (2007): Multiple correlation function approach: Rigorous results for simple geometries. Diff Fundam 5:1–34.

Hsu EW, Mori S (1995): Analytical expressions for the NMR apparent diffusion coefficients in an anisotropic system and a simplified method for determining fiber orientation. Magn Reson Med 34:194–200.

Jeurissen B, Leemans A, Jones DK, Tournier J-D, Sijbers J (2010a): Probabilistic fiber tracking using the residual bootstrap with constrained spherical deconvolution. Hum Brain Mapp 32:461–479.

Jeurissen B, Leemans A, Jones DK, Tournier JD, Sijbers J (2010b): Estimating the number of fiber orientations in diffusion MRI voxels: A constrained spherical deconvolution study. In: Proceedings 18th Scientific Meeting, International Society for Magnetic Resonance in Medicine, Stockholm, Sweden.

Jian B, Vemuri BC (2007): A unified computational framework for deconvolution to reconstruct multiple fibers from diffusion weighted MRI. IEEE Trans Med Imaging 26:1464–1471.

Jones DK (2008): Studying connections in the living human brain with diffusion MRI. Cortex 44:936–952.

Kaden E, Anwander A, Knösche TR (2008): Variational inference of the fiber orientation density using diffusion MR imaging. NeuroImage 42:1366–1380.

Leemans A, Jeurissen B, Sijbers J, Jones DK (2009): ExploreDTI: A graphical toolbox for processing, analyzing, and visualizing diffusion MR data. In: Proceedings 17th Scientific Meeting, International Society for Magnetic Resonance in Medicine, Hawaii, USA.

Nedjati-Gilani S, Parker GJ, Alexander DC (2006): Mapping the number of fibre orientations per voxel in diffusion MRI. In: Proceedings 14th Scientific Meeting, International Society for Magnetic Resonance in Medicine, Seattle, WA, USA.

Pannek K, Mathias JL, Bigler ED, Brown G, Taylor JD, Rose S (2010): An automated strategy for the delineation and parcellation of commissural pathways suitable for clinical populations utilising high angular resolution diffusion imaging tractography. NeuroImage 50:1044–1053.

Pierpaoli C, Jezzard P, Basser PJ, Barnett A, Di Chiro G (1996): Diffusion tensor MR imaging of the human brain. Radiology 201:637–648.

Raffelt D, Tournier JD, Rose S, Ridgway GR, Henderson R, Crozier S, Salvado O, Connelly A: Apparent fibre density: A novel measure for the analysis of diffusion-weighted magnetic resonance images. NeuroImage, doi:10.1016/j.neuroimage.2011.10.045.

Sakaie KE, Lowe MJ (2007): An objective method for regularization of fiber orientation distributions derived from diffusion-weighted MRI. NeuroImage 34:169–176.

Simmons A, Moore E, Williams SC (1999): Quality control for functional magnetic resonance imaging using automated data analysis and Shewhart charting. Magn Reson Med 41:1274–1278.

Smith SM, Jenkinson M, Woolrich MW, Beckmann CF, Behrens TE, Johansen-Berg H, Bannister PR, De Luca M, Drobnjak I, Flitney DE, Niazy RK, Saunders J, Vickers J, Zhang Y, De Stefano N, Brady JM, and Matthews PM. (2004): Advances in functional and structural MR image analysis and implementation as FSL. NeuroImage 23 (Suppl 1):S208–S219.

Smith SM, Jenkinson M, Johansen-Berg H, Rueckert D, Nichols TE, Mackay CE, Watkins KE, Ciccarelli O, Cader MZ, Matthews PM, Behrens TE (2006): Tract-based spatial statistics: Voxelwise analysis of multi-subject diffusion data. NeuroImage 31:1487–1505.

Tournier JD, Calamante F, Gadian DG, Connelly A (2004): Direct estimation of the fiber orientation density function from diffusion-weighted MRI data using spherical deconvolution. NeuroImage 23:1176–1185.

Tournier JD, Calamante F, Connelly A (2007): Robust determination of the fibre orientation distribution in diffusion MRI: Non-negativity constrained super-resolved spherical deconvolution. NeuroImage 35:1459–1472.

Tuch DS (2004): Q-ball imaging. Magn Reson Med 52:1358–1372.

van Gelderen P, DesPres D, van Zijl PC, Moonen CT (1994): Evaluation of restricted diffusion in cylinders. Phosphocreatine in rabbit leg muscle. J Magn Reson B 103:255–260.

Wang R, Benner T, Sorensen AG, Wedeen VJ (2007): Diffusion toolkit: A software package for diffusion imaging data processing and tractography. In: Proceedings 17th Scientific Meeting, International Society for Magnetic Resonance in Medicine, Berlin, Germany.

Waxman SG, Kocsis JD, Stys PK, editors (1995): The axon, structure, function and pathophysiology. Oxford University Press, New York, USA.

Wedeen VJ, Hagmann P, Tseng WY, Reese TG, Weisskoff RM (2005): Mapping complex tissue architecture with diffusion spectrum magnetic resonance imaging. Magn Reson Med 54:1377–1386.

Wedeen VJ, Wang R, Schmahmann J, Benner T (2008): Diffusion spectrum magnetic resonance imaging (DSI) tractography of crossing fibers. NeuroImage 41:1267–1277.

Wheeler-Kingshott C, Cercignani M (2009): About "axial" and "radial" diffusivities. Magn Reson Med 61:1255–1260.

Wiegell MR, Larsson HB, Wedeen VJ (2000): Fiber crossing in human brain depicted with diffusion tensor MR imaging. Radiology 217:897–903.

Wu Y-C, Alexander AL (2007): Hybrid diffusion imaging. NeuroImage 36:617–629.